Macroscale and microscale analyses of nitrification and denitrification in biofilms attached on membrane aerated biofilm reactors

Short running title: Nitrification in MABRs

By

HISASHI SATOH [1*], **HIDEKI ONO** [1], **BIAN RULIN** [2], **JYN KAMO** [3], **SATOSHI OKABE** [4] **and KEN-ICHI FUKUSHI** [1]

[1]*Department of Environmental and Civil Engineering, Hachinohe Institute of Technology, Hachinohe, Aomori 031-8501, Japan.*

[2]*School of Environmental Science and Technology, Tianjin University, Tianjin 300072, China.*

[3] *Mitsubishi Rayon Co., LTD., Nagoya 461-8677, Japan.*

[4]*Department of Urban and Environmental Engineering, Graduate school of Engineering, Hokkaido University, Sapporo 060-8628, Japan.*

- ** Corresponding Author*
  - *Hisashi SATOH*
  - *Department of Environmental and Civil Engineering, Hachinohe Institute of Technology, 88-1 Ohbiraki, Myo, Hachinohe, Aomori 031-8501, Japan.*
  - *Tel.: +81-(0)178-25-8067*
  - *Fax.: +81-(0)178-25-0722*
  - *E-mail: qsatoh@hi-tech.ac.jp*

Abstract

A membrane aerated biofilm reactor (MABR), in which O_2 was supplied from the bottom of the biofilm and NH_4^+ and organic carbon were supplied from the biofilm surface, was operated at different organic carbon loading rates and intra-membrane air pressures to investigate the occurrence of simultaneous COD removal, nitrification and denitrification. The spatial distribution of nitrification and denitrification zones in the biofilms was measured with microelectrodes for O_2, NH_4^+, NO_2^-, NO_3^- and pH. When the MABR was operated at approximately 1.0 g-COD/m^2/day of COD loading rate, simultaneous COD removal, nitrification and denitrification could be achieved. The COD loading rates and the intra-membrane air pressures applied in this study had no effect on the start-up and the maximum rates of NH_4^+ oxidation in the MABRs. Microelectrode measurements showed that O_2 was supplied from the bottom of the MABR biofilm and penetrated the whole biofilm. Because the biofilm thickness increased during the operations, an anoxic layer developed in the upper parts of the mature biofilms while an oxic layer was restricted to the deeper parts of the biofilms. The development of the anoxic zones in the biofilms coincided with increase in the denitrification rates. Nitrification occurred in the zones from membrane surface to a point of ca. 60 μm. Denitrification mainly occurred just above the nitrification zones. The COD loading rates and the intra-membrane air pressures applied in this study had no effect on location of the nitrification and denitrification zones.

Key words

Membrane aerated biofilm reactors; COD removal; Nitrification; Organic carbon loading rate; Intra-membrane air pressure; Microelectrodes

Introduction

Microbial nitrification is a key process in the removal of ammonia nitrogen from wastewater. The process of nitrification is carried out by ammonia-oxidizing and nitrite-oxidizing bacteria. Due to slow growth rates and the relatively high Km values to O_2 of nitrifying bacteria, nitrifying bacteria are generally outcompeted by heterotrophic bacteria for O_2 (Satoh et al., 2000). As a result, nitrification only occurs in conventional biofilm reactors when the organic carbon concentration is low.

A membrane aerated biofilm reactor (MABR) has been proposed as a promising alternative to the conventional biofilm reactors (Timberlake et al., 1988; Hibiya et al., 2003; Yamagiwa et al., 1994; Pankhania et al., 1994). In the MABR system, the biofilm develops on the outside surface of a hollow fiber membrane. O_2 is supplied from the inner side of the membrane to the bottom of the biofilm, whereas organic carbon in wastewater is supplied from the biofilm surface. Consequently, nitrification can occur at the bottom of the biofilm, where O_2 concentration is high and the organic carbon concentration is low due to diffusion limitation, resulting in the stable nitrification capacity of the reactor. Timberlake et al. (1988) reported that with combined organic carbon removal, nitrification and denitrification occurred simultaneously in the single MABR. They suggested that the occurrence of a vertical stratification of nitrification, aerobic heterotrophic oxidation, denitrification and anaerobic fermentation zones from the bottom to the surface of the biofilm. In practice, Hibiya et al. (2003) verified that ammonia-oxidizing bacteria were mainly distributed inside the biofilm and denitrifying bacteria were mainly distributed outside the biofilm in a MABR using the fluorescence *in situ* hybridization method. Furthermore, de Beer et al. (1997) was first to directly measure the nitrification and denitrification zones in the biofilm of a pilot-scale membrane reactor using microelectrodes. Such microscale information could be highly valuable when designing and operating MABRs. However, they did not investigate the effect of operating conditions of the MABR on the stratification of the microbial activity in the biofilm. Nitrogen and organic carbon loading rates, an intra-membrane air pressure, biomass retention time, and so on, should have significant effects of development of the stratification of the microbial activities in the MABR biofilm.

In this study, five types of a bench-scale MABR were operated at different chemical

oxygen demand (COD) loading rates and intra-membrane air pressures, and the performances of the MABRs were compared. The reaction rates of the MABR (i.e. macroscale activity) were monitored. Successive developments of oxic zones and spatial distributions of nitrification and denitrification zones in the biofilms (i.e. microscale activity) were investigated using O_2, NH_4^+, NO_2^-, NO_3^- and pH microelectrodes. The objectives of this study were to examine where nitrification occurred in the MABR biofilms achieving simultaneous COD removal, nitrification and denitrification, and the effects of operating conditions on the nitrification process in the biofilm on a macro- and microscale.

2. Materials and methods

2.1. Reactor operation

A MABR setup is presented schematically in Fig. 1. The reactor, which houses a membrane module, was constructed using an acrylic board. The cover of the reactor had openings for sample collection. The reactor volume including the recirculation line was 4.5 L. The membrane module consisted of gas permeable, polyurethane hollow fiber membranes. The inner and outer diameters of the hollow fiber are 237 μm and 275 μm, respectively. O_2 flux of the hollow fiber is 0.28 $m^3/m^2/h/MPa$. The membranes were arranged in parallel as a sheet (ca. 250 mm long and 300 mm wide) in the reactor with O_2 supplied via a manifold at the end of the membrane sheet. The other end of the membrane sheet was also connected to a manifold and the end of the manifold was open. The membrane surface area available for the biofilm attachment and oxygenation in the MABR was 0.25 m^2. The MABRs were each operated at 20 ± 1˚C, a constant dilution rate of 0.45 day^{-1} and a recirculation rate of 170 ml/s.

Five different types of biofilms were cultured in the bench scale MABRs. All biofilms were initially cultured in the batch-fed mode for three days with primary settling tank effluent (PSTE) provided by the Asahigaoka Domestic Wastewater Treatment Plant, Hachinohe, Japan. During the batch-fed cultivation period, the bulk liquid was completely withdrawn, and a fresh PSTE was filled daily. After initial cultivation with the PSTE, the MABR was operated in continuous flow mode with a synthetic medium. The medium

composition and operating conditions for each MABR are summarized in Table 1 and Table 2. The pH values in the influents were adjusted to 7.0 ± 0.1 for all the runs. O_2 concentrations in the medium were kept at 0 mg/L in the influent reservoir by pursing with N_2 gas. Air was pumped under a pressure of 0.01 or 0.04 MPa. The reaction rate of MABR was calculated using the following equation, $(C_{in} - C_{out}) \times Q / A$, where C_{in} is solute concentration in the influent, C_{out} is solute concentration in the effluent, Q is volumetric flow rate of the reactor and A is area of the membrane surface.

2.2. Microelectrode measurements and rate calculations

Clark-type microelectrodes for O_2 with tip diameters of approximately 15 μm were prepared and calibrated as described by Revsbech (1989). LIX-type microelectrodes for NH_4^+, NO_2^-, NO_3^- and pH with tip diameters of approximately 15 μm (de Beer et al., 1997) were constructed, calibrated, and used according to the reported protocol (Okabe et al., 1999). Microelectrode measurements of O_2 for *in situ* conditions were directly performed in the MABRs at regular time intervals under actual growth conditions during operations. The microelectrode was introduced into the MABR through the sampling opening. When the microprofiles of O_2, NH_4^+, NO_2^-, NO_3^- and pH in the biofilm were measured, the bulk liquid in the MABR was exchanged for a synthetic medium. The medium that was used to monitor the concentration profiles consisted of NH_4Cl (16 mg-N/L), $NaNO_2$ (7 mg-N/L), $NaNO_3$ (25 mg-N/L), Na_2HPO_4 (81 mg/L), $MgCl_2 \cdot 6H_2O$ (17 mg/L), $CaCl_2$ (22 mg/L), and EDTA (100 mg/L). The biofilm was acclimated in the medium for microelectrode measurements with less than 1 mg/L of O_2 and at 20˚C for at least two hours before measurement, to ensure that steady-state profiles were obtained. The concentration profiles in the biofilm were recorded using a motor-driven micromanipulator at intervals of 20 to 100 μm from the bulk liquid into the biofilm (Satoh et al., 2003). The membrane surface was considered as the point where solute concentrations were unchanged in the biofilm.

Net specific consumption rates of NH_4^+, NO_2^- and NO_3^- were estimated from the mean concentration profiles by using Fick's second law of diffusion, $\partial C(z,t)/\partial t = D \times \partial^2 C(z,t)/\partial z^2 - R(z)$, where C(z,t) is the concentration at time t and depth z, D is the molecular diffusion coefficient in the liquid phase, R is the net specific consumption rate. After integration of

this equation, we have $C_{n-1} = C_n + h \times [dC/dz_{n-1} + h \times A_{n-1}]$, where Cn is the concentration measured with a microelectrode at n time, h is the step size of microelectrode measurement and $A_n = R_n/D$. Using this equation, we can calculate concentration profiles by altering these net activities and minimizing the sum of squared deviations of the calculated profile from the measured profile. We chose to use Microsoft EXCEL Solver to achieve this goal. The details of this method have been described previously by Lorenzen et al. (1998). Furthermore, the total nitrification rate [J; g-N/m^2/day] of the biofilm was calculated using Fick's first law of diffusion, J = -Ds (dCs/dz), where dCs/dz is the measured concentration gradient of each solute in the boundary layer at the biofilm-liquid interface. Molecular diffusion coefficients of 1.38×10^{-5} cm^2/s for NH_4^+, 1.23×10^{-5} cm^2/s for NO_2^- and 1.23×10^{-5} cm^2/s for NO_3^- at 20˚C were used for the calculations, respectively (Andrussow, 1969).

2.3. Analytical methods

The NH_4^+ and NO_2^- concentrations were determined colorimetrically. The NO_3^- concentration was determined using an ion chromatograph (HIC-6A; Shimadzu) equipped with a Shim-pack IC-A1 column. The samples for NH_4^+, NO_2^- and NO_3^- were filtered with 0.45 μm membrane filters before analysis. COD was analyzed using $KMnO_4$ according to the standard methods (APHA, 1998). Total nitrogen (TN) was analyzed colorimetrically with potassium peroxodisulfate. The O_2 concentration and pH were determined using an O_2 electrode and a pH electrode, respectively.

3. Results and discussion

3.1. Reactor performance

When the MABR was operated at a high COD loading rate (run-1), a thick and brownish biofilm developed. Microelectrode measurements revealed that biofilm thickness was ca. 3 mm. NH_4^+ concentrations in the effluent were higher than in the influent during the more than 60 days of operation (data not shown). This was probably explained by the degradation of yeast extract to NH_4^+ and low NH_4^+ oxidation rate due to a low

intra-membrane air pressure. Fig.2 shows the influent and effluent concentrations of NH_4^+, NO_2^-, NO_3^- and COD, and O_2 concentrations in the MABRs in run-2 to run-5. Fig.3 shows development of NH_4^+, NO_2^-, COD and total nitrogen removal rates of the MABRs in run-2 to run-5. When the MABRs were operated at lower COD loading rates (run-2 to run-5), the biofilms had a fluffy structure and were brownish in color. The thickness of the biofilms was less than 2.1 mm (Fig. 4). Visual observations indicated that the biofilm attachment areas accounted for about half of the total membrane surface area on day 40 during run-2 to run-5. Therefore, O_2 diffused directly into the bulk liquid without utilization by microorganisms in the biofilm. O_2 concentrations in the bulk liquid fluctuated between 0 and 2 mg/L (Fig. 2I). The partial attachment of the biofilm might be explained by low organic carbon loading rate and sloughing of the biofilm due to liquid flow in the reactor and air pressure from the bottom of the biofilm. NH_4^+ oxidation occurred immediately after switching to the continuous-feed operation on day 0 and reached maximum rates within 10 days during run-2 to run-5 (Fig. 3A). NO_2^- oxidation was achieved within 30 days (Fig. 3B). Consequently, we can conclude that the intra-membrane air pressures applied in this study had no effect on the start-up and the maximum rates of nitrification in the MABRs at a low COD loading rate, whereas at a high COD loading rate the MABR had to be operated with a high intra-membrane air pressure for stable nitrification. A possible explanation for the complete nitrification at the low intra-membrane air pressure is that nitrification occurred in the deeper parts of the biofilms, as discussed below.

COD removal rates were less than 0.15 g-COD/m^2/day (corresponding to ca. 60% COD removal) in run-1 and run-2 (Fig. 3C). These low rates were due to fluctuations in the COD loading rate. In contrast, the COD removal rates increased during start-up periods and reached rates of ca. 1.0 g-COD/m^2/day (corresponding to ca. 90% COD removal) after 17 days in run-4 and run-5. Consequently, simultaneous organic carbon removal and nitrification were achieved in run-4 and run-5.

The rates of organic carbon removal and nitrification for the various types of MABRs are summarized in Table 3. Yamagiwa et al. (1994) reported the simultaneous occurrence of organic carbon removal and nitrification by the biofilm that was formed on an O_2 enrichment-type support. The higher rates of organic carbon removal and nitrification could be attributed to accumulation of microorganisms in a fibrous support woven around the fiber.

In contrast, nitrification rates were lower with the laboratory scale permeable-support biofilm reactor (Timberlake et al., 1988) and the laboratory scale hollow fiber membrane bioreactor (Pankhania et al., 1994), although organic carbon removal was achieved. This was attributed to either a low pH, a short retention time of biomass by backwashing, a mass transfer limitation due to a thicker biofilm, or the lack of fully developed nitrification zones. Therefore, simultaneous occurrence of organic carbon removal and nitrification in this study could be a result of lower organic carbon loading rates and operation without backwashing.

In addition to organic carbon removal and nitrification, total nitrogen (TN) removal occurred, although the rates were lower than the nitrification rates (Fig. 3D). TN removal rates on day 40 were ranged from 0.12 to 0.33 g-N/m^2/day for run-2 through run-5. TN removal is usually attributed to denitrification and bacterial assimilation. It was possible that denitrification occurred in the floc present in the bulk liquid.

3.2. O_2 microprofiles in the biofilms under in situ *conditions*

O_2 microprofiles in the biofilms were directly measured under *in situ* conditions at different stages of biofilm development in run-4 and run-5. Fig. 4 shows the mean values of more than three O_2 profiles measured at different positions and average biofilm thickness, except that at day 7, at which a typical profile is displayed. The biofilm thickness increased from ca. 100 μm on day 7 to ca. 1,200 μm at day 51 in run-4. During the operation at a high intra-membrane air pressure (i.e. run-5) the biofilm thickness increased from ca. 200 μm on day 7 to ca. 2,100 μm on day 51.

O_2 concentration was highest at the membrane surface in all stages of biofilm development, indicating that O_2 was diffused through the membrane. O_2 concentrations decreased in the direction from the membrane to the bulk liquid. O_2 penetrated the whole biofilm and diffused out of the biofilms until day 23 in run-4. On day 29, the anoxic zones were first detected in the upper parts of the biofilm. In this case, a trace amount of O_2 present in the bulk liquid as well as the O_2 supplied from the membrane was utilized. In run-5, the anoxic zones were first detected on day 37. Since the biofilm thickness increased thereafter without obvious sloughing, the anoxic zones expanded. The development of anoxic zones in

the biofilms coincided with the increase in the TN removal rates (i.e. denitrification rates) after day 37 and day 41 in run-4 and run-5, respectively (Fig. 3D).

The O_2 concentrations at the membrane surface ranged between 1.7 - 4.7 and 1.3 - 4.8 mg/L in run-4 and run-5, respectively. The O_2 concentrations at 20˚C and air pressure below 0.01 and 0.04 MPa are theoretically 0.9 and 3.5 mg/L, respectively. The O_2 concentrations at the membrane surface were not constant during operations of both runs, and the higher intra-membrane air pressure did not result in the higher O_2 concentration at the membrane surface. The fluctuation of intra-membrane air pressure was in the range of 0.005 MPa. The fluctuation of O_2 concentrations might result from clogging of the membrane during operation (Timberlake et al., 1988), spatial heterogeneity of pore size throughout the membrane (Kosutic et al., 2000), and the partial attachment of the biofilm onto the membrane surface.

3.3. Microprofiles of O_2, NH_4^+, NO_2^-, NO_3^- and pH in the biofilms measured in the medium for microelectrode measurements

O_2, NH_4^+, NO_2^-, NO_3^- and pH microprofiles in the biofilms in run-2, run-4 and run-5 were measured at 30, 32 and 38 days, respectively (Fig. 5), and the net specific consumption rates of NH_4^+, NO_2^- and NO_3^- were estimated on the basis of the measured profiles (Fig. 6). These results represent the potential nitrification capacity of the biofilms in the MABRs because no organic carbon was added to the medium for microelectrode measurements. In contrast to the measurements under *in situ* conditions (Fig 4), O_2 was not depleted in all biofilms (Fig. 5). This was probably due to the absence of organic carbon in the medium for microelectrode measurements. Nitrification was detected in the zones from membrane surface to a point of ca. 60 μm in run-2, run-4 and run-5. In contrast, since O_2, NH_4^+ and organic carbon are supplied from one side of the biofilm in the conventional biofilm reactors, the oxic zones are restricted to the upper parts of the biofilm (Okabe et al., 1999; Schramm et al., 1996). From these results, we can conclude that O_2 supplied from the bottom of the biofilm using a gas permeable membrane results in the development of a nitrifying layer in the deeper parts of the biofilm. This unique distribution of an active nitrifying layer in the MABR biofilm has several advantages over the conventional biofilm reactors (Timberlake

et al., 1988): (i) nitrifying bacteria in the MABR were present under the favorable condition in which O_2 concentrations were high while organic carbon concentration was low. In contrast, in the conventional biofilm reactor autotrophic nitrifying bacteria are excluded from the upper oxic layer of the biofilm due to the faster growth of heterotrophic bacteria, which often leads to deterioration of nitrification (Satoh et al., 2000); (ii) nitrifying bacteria, which usually showed slow growth rates and high sensitivity to several environmental factors, were immobilized in the deeper parts of the biofilm, and they were thus protected from toxic shocks and detachment losses by sloughing.

Denitrification mainly occurred just above the nitrification zones. The close vicinity of nitrification and denitrification zones enhanced denitrification, because NO_3^-, produced in the deeper parts of the biofilm, diffused through the anoxic parts of the biofilm that had high organic carbon content. The COD loading rates and the intra-membrane air pressures under the conditions of run-2, run-4 and run-5 had no effect on the location of the nitrification and denitrification zones. This result might explain that the intra-membrane air pressures applied in this study had no effect on the NH_4^+ oxidation rates in the MABRs at a low COD loading rate (Fig. 3).

Conclusions

(1) Simultaneous COD removal, nitrification and denitrification could be achieved in the MABRs. The efficiencies of nitrification and COD removal were 95% and 90%, respectively. The intra-membrane air pressures applied in this study had no effect on the start-up and the maximum rates of NH_4^+ oxidation in the MABRs at a low COD loading rate, whereas at a high COD loading rate the MABR had to be operated with a high intra-membrane air pressure for stable nitrification.

(2) Microelectrode measurements directly revealed O_2 profiles in the MABR biofilms. O_2 was diffused through the membrane and utilized by microorganisms in the biofilm. The development of anoxic zones in the biofilms coincided with the increase in the denitrification rates of the MABRs.

(3) Microelectrode measurements of O_2, NH_4^+, NO_2^-, NO_3^- and pH in the biofilms demonstrated that nitrification occurred in the zones from membrane surface to a point of ca.

60 μm and denitrification mainly occurred just above the nitrification zones. The low COD loading rates (<1.1 g-COD/m^2/day) and the intra-membrane air pressures (0.01 and 0.04 MPa) had no effect on the location of the nitrification and denitrification zones.

References

Andrussow, L. (1969) Diffusion. In *Landolt-Bornstein Zahlenwerte und Functionen. vol. II/5a*, eds. Borchers H., Hauser H., Hellwege K. H., Schafer K. and Schmidt E. Springer, Berlin, Germany.

APHA, AWWA and WEF. (1998) *Standard Methods for the examination of water and wastewater* (20th edn.). American Public Health Association, Washington, DC.

de Beer, D., Schramm, A., Santegoeds, C. M. and Kuhl, M. (1997) A nitrite microsensor for profiling environmental biofilms. *Applied and Environmental Microbiology* **63**(3), 973-977.

Hibiya, K., Terada, A., Tsuneda, S. and Hirata, A. (2003) Simultaneous nitrification and denitrification by controlling vertical and horizontal microenvironment in a membrane-aerated biofilm reactor. *Journal of Biotechnology* **100**, 23-32.

Kosutic, K., Kastelan-Kunst, L. and Kunst, B. (2000) Porosity of some commercial reverse osmosis and nanofiltration polyamide thin-film composite membranes. *Journal of Membrane Science* **168**, 101-108.

Lorenzen, J., Larsen, L. H., Kjær, T. and Revsbech, N. P. (1998) Biosensor determination of the microscale distribution of nitrate, nitrate assimilation, nitrification, and denitrification in a diatom-inhabited freshwater sediment. *Applied and Environmental Microbiology* **64**(9), 3264-3269.

Okabe, S., Satoh, H. and Watanabe, Y. (1999) In situ analysis of nitrifying biofilms as determined by in situ hybridization and the use of microelectrodes. *Applied and Environmental Microbiology* **65**(7), 3182-3191.

Pankhania, M., Stephenson, T. and Semmens, M. J. (1994) Hollow fibre bioreactor for wastewater treatment using bubbleless membrane aeration. *Water Research* **28**(10), 2233-2236.

Revsbech, N. P. (1989) An oxygen microelectrode with a guard cathode. *Limnology and Oceanography* **34**, 474-478.

Satoh, H., Nakamura, Y., Ono, H. and Okabe, S. (2003) Effect of oxygen concentration on nitrification and denitrification in single activated sludge flocs. *Biotechnology and Bioengineering* **83**(5), 604-607.

Satoh, H., Okabe, S., Norimatsu, N. and Watanabe, Y. (2000) Significance of substrate C/N ratio on structure and activity of nitrifying biofilms determined by *in situ* hybridization and the use of microelectrodes. *Water Science and Technology* **41**(4-5), 317-321.

Schramm, A., Larsen, L. H., Revsbech, N. P., Ramsing, N. B., Amann, R. and Schleifer, K.-H. (1996) Structure and function of a nitrifying biofilm as determined by *in situ* hybridization and the use of microelectrodes. *Applied and Environmental Microbiology* **62**(12), 4641-4647.

Timberlake, D. L., Strand, S. E. and Williamson, K. J. (1988) Combined aerobic heterotrophic oxidation, nitrification and denitrification in a permeable-support biofilm. *Water Research* **22**(12), 1513-1517.

Yamagiwa, K., Ohkawa, A. and Hirasa, O. (1994) Simultaneous organic carbon removal and nitrification by biofilm formed on oxygen enrichment membrane. *Journal of Chemical Engineering of Japan* **27**(5), 638-643.

List of Figures

biofilm is indicated by the gray area.

Fig. 6. The spatial distribution of the net specific consumption rates of NH_4^+ (●), NO_2^- (+) and NO_3^- (□) in the MABR biofilms in run-2, run-4 and run-5 at 30 days, 32 days and 38 days, respectively. The membrane surface is at a depth of 0 μm. The biofilm is indicated by the gray area.

Run	NH_4Cl (g-N/L)	$NaHCO_3$ (g/L)	$KHCO_3$ (g/L)	K_2HPO_4 (g/L)	$CaCl_2$ (g/L)	$MgCl_2 \cdot 6H_2O$ (g/L)	Yeast extract (g/L)
1	0.1	0.63	0.91	0.22	0.08	0.70	1.0
2	0.1	0.63	0.91	0.22	0.08	0.70	0.1
3	0.1	0.63	0.91	0.22	0.08	0.70	0.1
4	0.1	0.63	0.91	0.22	0.08	0.70	0.5
5	0.1	0.63	0.91	0.22	0.08	0.70	0.5

Table.1
Macroscale and microscale analyses of nitrification and denitrification in biofilms attached on membrane aerated biofilm reactors.
Hisashi Satoh et al.

Run	COD loading rate (g-COD/m^2/day)	Total nitrogen loading rate (g-N/m^2/day)	NH_4^+ loading rate (g-N/m^2/day)	Intra-membrane air pressure (MPa)
1	1.8 ± 0.3	N.D.[a]	0.46 ± 0.17	0.01
2	0.20 ± 0.10	0.73 ± 0.11	0.47 ± 0.09	0.01
3	0.19 ± 0.12	0.72 ± 0.10	0.54 ± 0.09	0.04
4	1.1 ± 0.4	1.0 ± 0.2	0.58 ± 0.08	0.01
5	1.0 ± 0.3	1.1 ± 0.1	0.59 ± 0.05	0.04

[a] Not determined.

Table.2
Macroscale and microscale analyses of nitrification and denitrification in biofilms attached on membrane aerated biofilm reactors.
Hisashi Satoh et al.

Organic carbon loading rate ($g/m^2/day$)	Total nitrogen loading rate ($g\text{-}N/m^2/day$)	Organic carbon removal rate ($g/m^2/day$)	Nitrification rate ($g\text{-}N/m^2/day$)	Reference
1.2 - 1.5 (as COD)	1.0 - 1.2	1.1 - 1.4 (as COD)	0.5	This paper
6.6 (as TOC)	2.4	6.3 (as TOC)	1.7 - 2.2	[4]
3.4 - 10.8 (as TOC)	1.7 - 6.5	1.9 - 4.4 (as TOC)	-0.01 - 0.03 [a]	[2]
1.24 - 1.75 (as COD)	0.21 - 0.3	0.82 - 1.50 (as COD)	No nitrification	[5]

[a] NO_3^- production rate.

Table.3
Macroscale and microscale analyses of nitrification and denitrification in biofilms attached on membrane aerated biofilm reactors.
Hisashi Satoh et al.

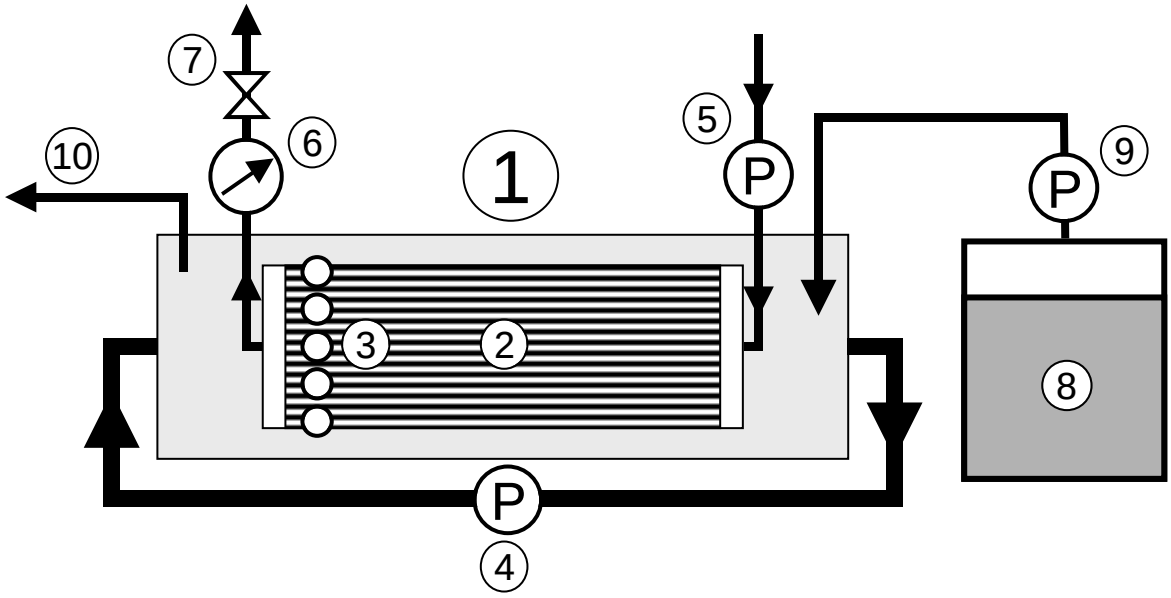

Fig.1
Macroscale and microscale analyses of nitrification and denitrification in biofilms attached on membrane aerated biofilm reactors.
Hisashi Satoh et al.

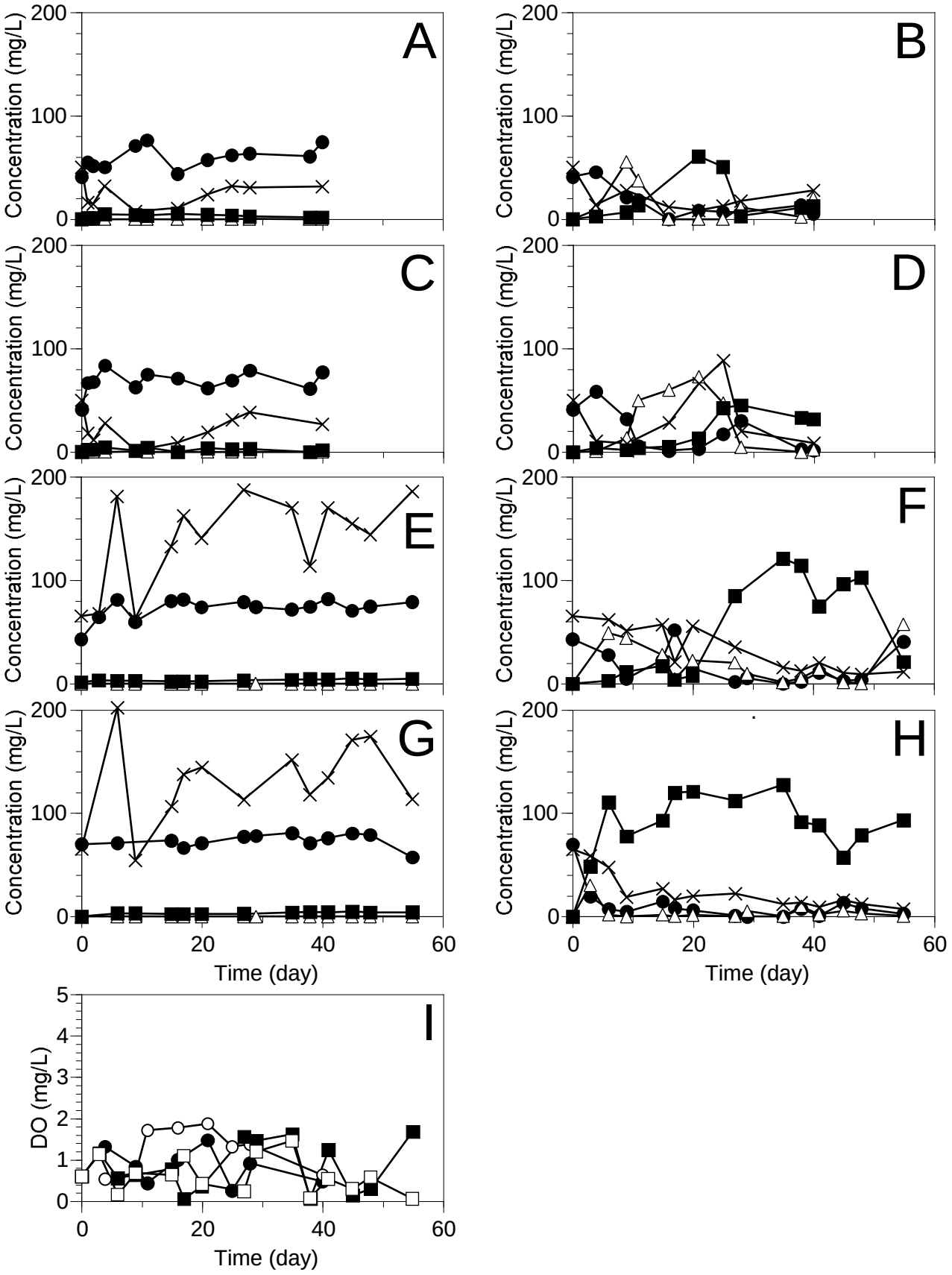

Fig.2
Macroscale and microscale analyses of nitrification and denitrification in biofilms attached on membrane aerated biofilm reactors.
Hisashi Satoh et al.

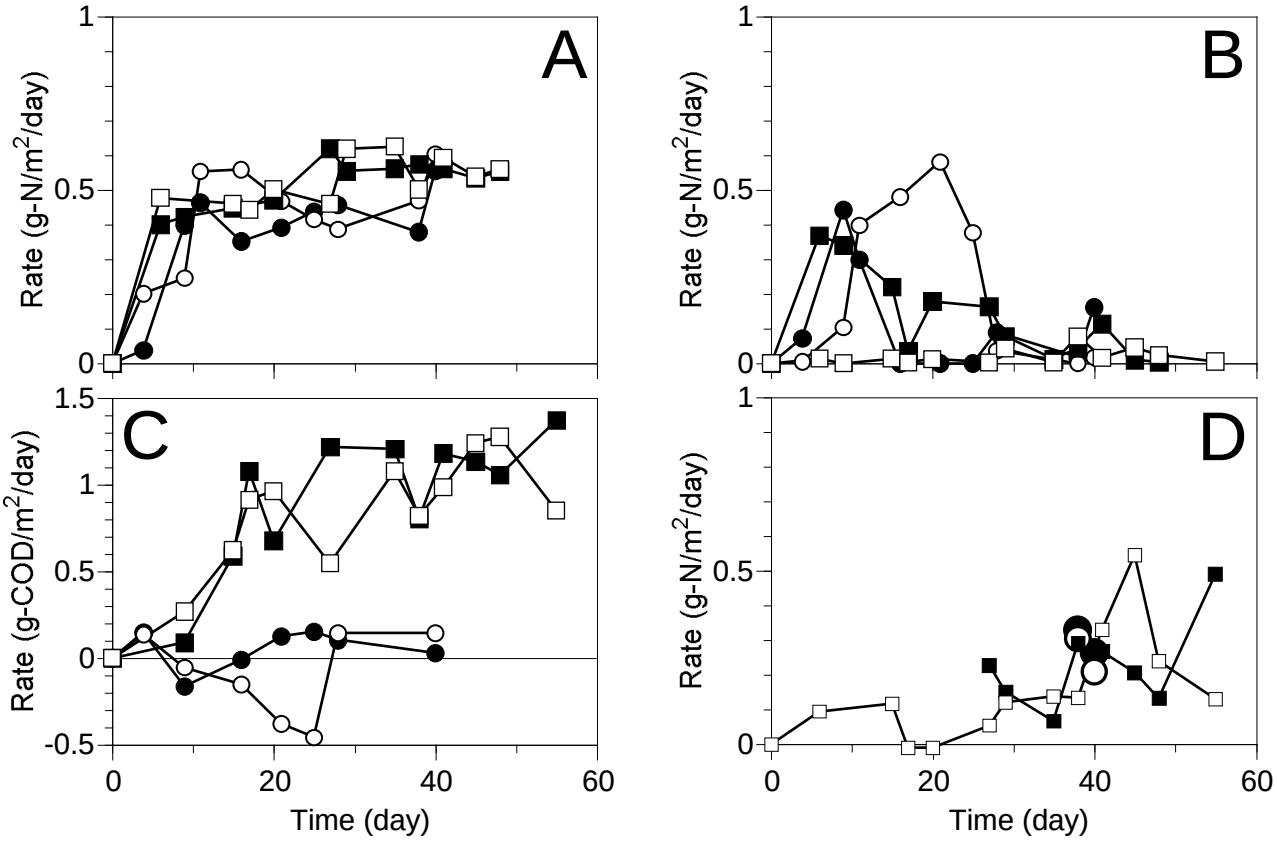

Fig.3
Macroscale and microscale analyses of nitrification and denitrification in biofilms attached on membrane aerated biofilm reactors.
Hisashi Satoh et al.

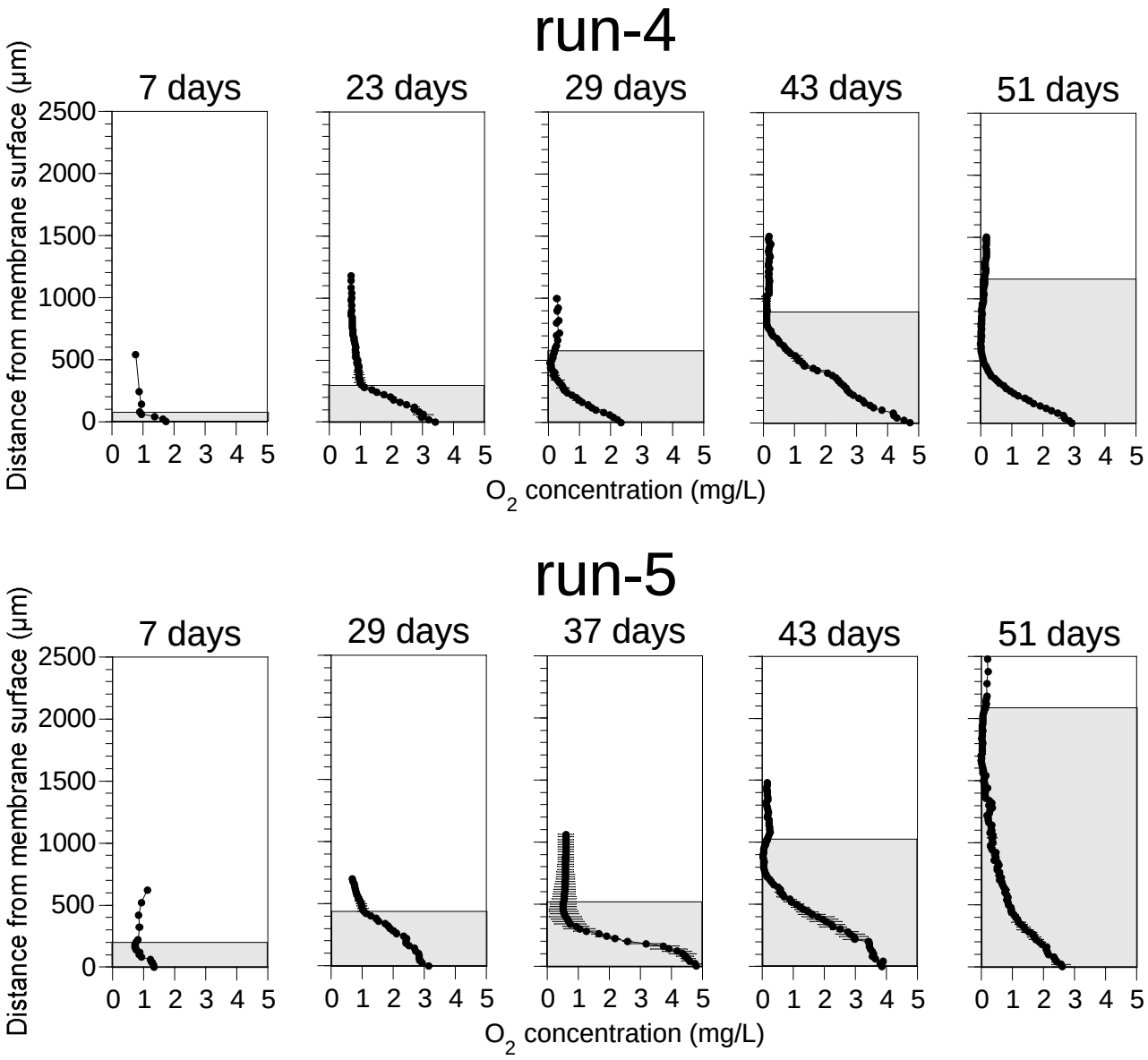

Fig.4
Macroscale and microscale analyses of nitrification and denitrification in biofilms attached on membrane aerated biofilm reactors.
Hisashi Satoh et al.

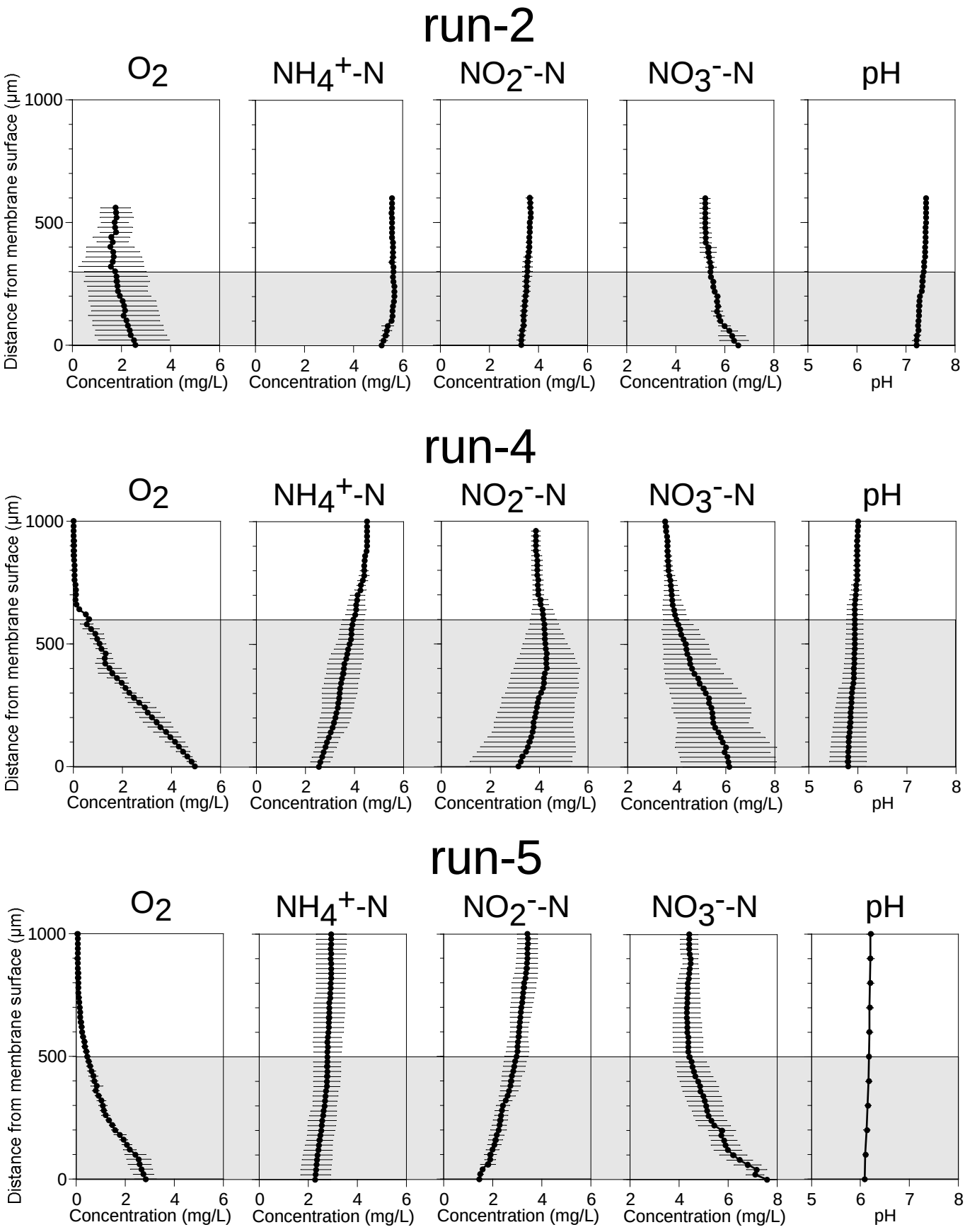

Fig.5
Macroscale and microscale analyses of nitrification and denitrification in biofilms attached on membrane aerated biofilm reactors.
Hisashi Satoh et al.

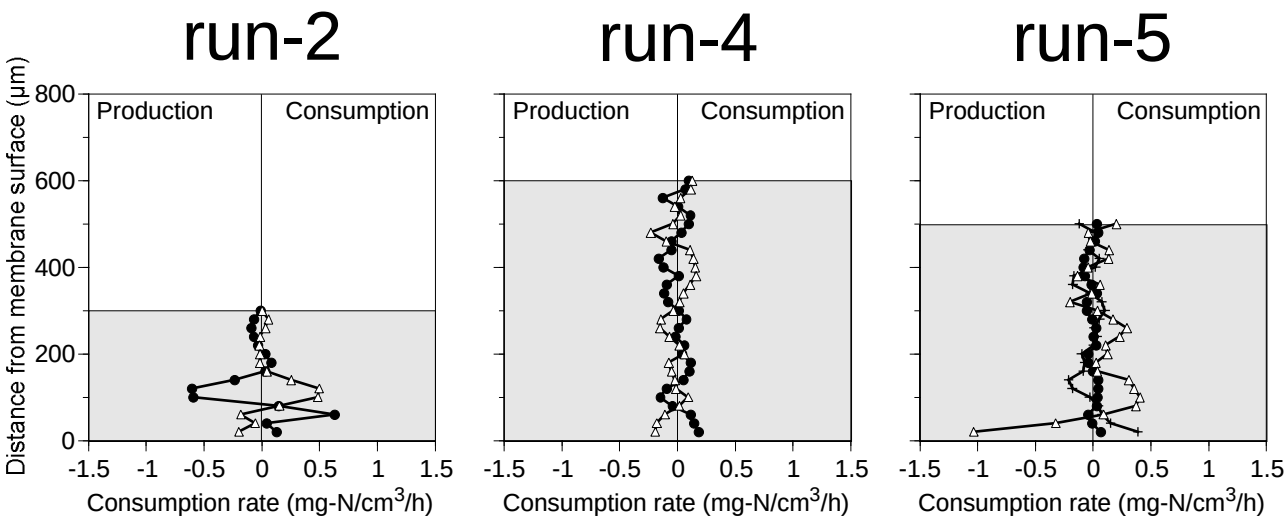

Fig.6
Macroscale and microscale analyses of nitrification and denitrification in biofilms attached on membrane aerated biofilm reactors.
Hisashi Satoh et al.